I&EC research
Industrial & Engineering Chemistry Research

Article

pubs.acs.org/IECR

CO_2 Dissolution and Design Aspects of a Multiorifice Oscillatory Baffled Column

Filipa M. Pereira,[†] Diana Z. Sousa,[†] M. Madalena Alves,[†] Malcolm R. Mackley,[‡] and Nuno M. Reis*[,‡,§]

[†]IBB - Institute for Biotechnology and Bioengineering, Centre of Biological Engineering, Universidade do Minho, Campus de Gualtar, 4710-057 Braga, Portugal

[‡]Department of Chemical Engineering and Biotechnology, University of Cambridge, New Museum Site, Pembroke Street, CB2 3RA Cambridge, U.K.

[§]Department of Chemical Engineering, Loughborough University, Loughborough LE11 3TU, U.K.

Supporting Information

ABSTRACT: Dissolution of CO_2 in water was studied for a batch vertical multiorifice baffled column (MOBC) with varying orifice diameters (d_0) of 6.4−30 mm and baffle open area (α) of 15−42%. Bubble size distributions (BSDs) and the overall volumetric CO_2 mass transfer coefficient (K_La) were experimentally evaluated for very low superficial gas velocities, U_G of 0.12−0.81 mm s^{-1}, using 5% v/v CO_2 in the inlet gas stream at a range of fluid oscillations (f = 0−10 Hz and x_0 = 0−10 mm). Remarkably, baffles presenting large d_o = 30 mm and α = 36%, therefore in the range typically found for single-orifice oscillatory baffled columns, were outperformed with respect to BSD control and CO_2 dissolution by the other baffle designs or the same aerated column operating without baffles or fluid oscillations. Flow visualization and bubble tracking experiments also presented in this study established that a small d_o of 10.5 mm combined with a small value of α = 15% generates sufficient, strong eddy mixing capable of generating and trapping an extremely large fraction of microbubbles in the MOBC. This resulted in increased interfacial area yielding K_La values up to 65 ± 12 h^{-1} in the range of the U_G tested, representing up to 3-fold increase in the rate of CO_2 dissolution when compared to the unbaffled, steady column. In addition, a modified oscillatory Reynolds number, Re_o' and Strouhal number, St' were presented to assist on the design and scale-up of gas−liquid systems based on multiorifice oscillatory baffled columns. This work is relevant to gas−liquid or multiphase chemical and biological systems relying on efficient dissolution of gaseous compounds into a liquid medium.

1. INTRODUCTION

The sequestration of carbon dioxide (CO_2) is a topic of major industrial interest motivated by the recent increased need for reducing the greenhouse gas emissions. New biotechnological processes are being developed where microalgae, anaerobic bacteria, or cyanobacteria use CO_2 to produce bulk chemicals and green fuels.[1−3] The intensification of dissolution of CO_2 and other gases requires generating fine bubbles and reducing the mass transfer resistances around the bubbles surface by means of strong mechanical mixing using, for example, a mechanical impeller, which is not always possible in biological processes involving living cells as the external energy input must also ensure cell integrity.[4,5]

Conventional gas−liquid contacting technology based on, for example, bubble columns (BCs), stirred tank reactors (STRs), and air-lift reactors (ALRs) are somewhat inefficient and present very modest performances[6] with respect to the dissolution of gases with large gas aeration rates (Q_{gas}) of 1 vvm (volume of gas per volume of liquid per minute) or above; in the particular case of BCs and ALRs this is due to the intensity of mixing being directly linked to the gas flow rates, the contacting times, therefore, being extremely short.

The overall volumetric mass transfer coefficient (K_La) for CO_2 has been experimentally measured only in a small number of studies.[7−10] Calderbank and Lochiel[7] investigated K_La, the bubble's velocity, and shape for CO_2 freely rising in distilled water and showed that K_La remained constant along the height of the column for bubbles with an equivalent spherical diameter d_e in the range 4−31 mm. Boogerd and coauthors[8] showed that K_La for CO_2 can be predicted from the known K_La values measured for O_2, using the following relation: $K_La_{,CO2}$ = 0.893×$K_La_{,O2}$ which has been derived from a diffusion coefficient correction factor. On the basis of that same relationship these authors have predicted a maximum possible K_La value for CO_2 in the order of 140 h^{-1}, based on K_La values measured for O_2 at a Q_{gas} = 1 vvm in a lab-scale fermenter operating at pH = 2, which has yet to be demonstrated experimentally. Hill[10] determined the dependence of K_La for CO_2 with the temperature, stirring speed, and Q_{gas} = 0.08−0.8 vvm in a 2.45 L STR filled with distilled water and obtained K_La values of 20−120 h^{-1} using a 10% v/v CO_2, well below the typical K_La values measured for O_2−water mass transfer in well-mixed vessels. It is however unclear from that study what were the specific conditions that allowed Hill[10] to achieve the highest K_La values reported. Nevertheless, this stresses the difficulty in predicting or comparing performance of different gas contacting systems in respect to CO_2 dissolution.

The oscillatory baffled column (OBC)[11] is a new mixing technology that has been successfully applied to the

Received: October 7, 2013
Revised: September 11, 2014
Accepted: October 6, 2014
Published: October 6, 2014

Table 1. Gas−Liquid Mass Transfer Studies in Oscillatory Baffled Columns (OBCs)

OBC	gas−liquid system	i.d. [mm]	Q_{gas} [vvm]	U_G [mm s^{-1}]	d_o [mm]	α [%]	K_La [h^{-1}]	ref
batch single-orifice OBC	air−fermentation media	50	0.5	3.2	20[a]	16	∼90−450	Ni et al.[22]
batch reciprocating plate baffled column	air−water (self-aerating)	190	n/a	n/a	10−50	7−31	∼0−23	Mackley et al.[14]
batch reciprocating plate baffled column	air−water	150	n/d	0.32−1.14	70−90	22−36	n/a	Baird et al.[12]
batch reciprocating plate baffled column	air−water	16.6	n/d	5−15	7.8	46.6	180−2880	Vasic et al.[24]
batch reciprocating plate baffled column	air−water	228	n/d	1.2−11.8	6.4−19.1	31.2−35.7	∼20−720	Gagnon et al.[6]
batch single-orifice OBC	air−water	50	0.05−0.2	1.1−4.3	24	23	∼0−144	Oliveira and Ni[27,31]
batch single-orifice OBC	air−water	26	n/d	0.4−2.4	15	33	∼0−133	Hewgill et al.[13]
batch single-orifice OBC	ozone−water	25	n/d	3−68	12.5	25	36−252	Al-Abduly et al.[34]
continuous dual-reciprocating plate baffled column	air−water	100	n/d	0−1700	1.6−3.2	38	∼72−432	Gomaa et al.[33]
continuous reciprocating plate baffled column	air−water	150	n/d	6.3−17.7	6.4−90	23.5−54	∼7−54	Rama Rao and Baird[19]
continuous single-orifice OBC	pure CO_2−water	94	1.3−3.6	26−72	50	28	∼8−100	Taslim and Trakriff[9]
continuous, single-orifice meso-OBC	air−water	4.4	0.064	0.37	1.6	14	∼0−576	Reis et al.[30]

[a]Authors reported a baffles width/diameter of 30 mm, so it was assumed an open orifice diameter of 20 mm in the calculations; (n/d) not disclosed by the authors; (n/a) not applicable/available.

intensification of a wide range of chemical and biological processes, including gas−liquid and multiphase systems. The eddy mixing in the periodic baffles or constrictions delivers a good degree of radial mixing and secondary flow that is very effective for controlling the bubble/drop size distribution in the column enhancing the contact between immiscible phases. Few studies have previously used OBCs for O_2 and CO_2 dissolution in water,[9,12−19] all based on single-orifice OBCs as overviewed in Table 1. Reis et al.[20] reported values of K_La up to 576 h^{-1} for O_2 dissolution in a meso-OBC using the very low value for superficial gas velocity (U_G) of 0.37 mm s^{-1} (equivalent to Q_{gas} = 0.064 vvm). The superior gas−liquid performance of the meso-OBC resulted mainly from the enhanced gas hold-ups associated with the trapping of microbubbles in the periodic eddies generated in the space between the narrow constrictions, as well as the enhanced shear and velocity fluctuations in the gas−liquid interface. Only on one was occasion the dissolution of CO_2 has been experimentally studied in OBCs, but in this instance pure CO_2 in a continuous 94 mm i.d. column was used by Taslim and Takriff;[9] K_La values up to ∼100 h^{-1} were reported for Q_{gas} = 1.3−3.6 vvm. Overall, OBCs are very efficient in respect to gas−liquid mass transport, and the large values of K_La reported were obtained with a 5- to 10-fold reduction in Q_{gas} when compared to the gas aeration rates typically used for BCs, ALRs, or STRs. An additional feature perhaps unique to OBCs is its linear scale-up in some particular applications;[15,21−23] however, no rules have yet been established with respect to the scale-up of gas−liquid mixing in OBCs.

In this work, the dissolution of CO_2 on a vertical 150 mm i.d. batch multiorifice baffled column (MOBC) was experimentally studied and three baffle configurations with different open area (α) and orifice diameter (d_0) were developed and tested. The impact of baffle design and Q_{gas} on K_La was quantitatively evaluated. Optical flow visualization and image analysis were applied for quantifying the impact of oscillatory flow mixing on the Sauter mean diameter ($D_{3,2}$) and BSDs. For the first time the connection between microbubbles trapping and the toroidal vortices in OBCs is quantitatively illustrated. In addition, the main governing dimensionless numbers used for characterizing the oscillatory flow mixing intensity were revisited, which should establish the principles for the design of MOBC and scale-up from single-orifice to multiorifice OBCs.

2. EXPERIMENTAL METHODS AND PROCEDURES

2.1. Multiorifice Oscillatory Baffled Column (MOBC).

The 150 mm internal diameter MOBC used in this work is presented in Figure 1. The total volume of the column was 10.6 L, with a working volume (V_L) of 9.6 L, and a total column height (h) of 540 mm. All experiments have been carried out at atmospheric pressure and room temperature (20 °C).

The gas phase consisted of 5% v/v of CO_2 in air sparged from the bottom of the MOBC. The composition of the gas phase was chosen to prevent changes in the bubbles size due to CO_2 absorption and to minimize the effect of response time of the dissolved CO_2 probe. The sparger consisted of a circular plastic tube perforated with a 0.6 mm diameter needle to deliver an even bubble formation within the column. Q_{gas} was controlled by a needle valve and measured with a calibrated in-line gas flow meter. The range of Q_{gas} values herein tested was 0.01−0.1 vvm, corresponding to a range of U_G of 0.12−0.81 mm s^{-1}.

The liquid phase (distilled water) in the MOBC was kept at a constant volume, with the free liquid surface always kept well above the top baffle in order to avoid air entrapment from the headspace. Sinusoidal fluid oscillations were imposed on the fluid using a servo-hydraulic system that controlled a 125 mm o.d. piston attached to the bottom of the column. This moving base piston was capable of delivering fluid oscillation frequency (f) and center-to-peak amplitude (x_0) in the ranges of 0−10 Hz and 0−10 mm, respectively. Because of the nature of design of

dx.doi.org/10.1021/ie403348g | Ind. Eng. Chem. Res. 2014, 53, 17303−17316

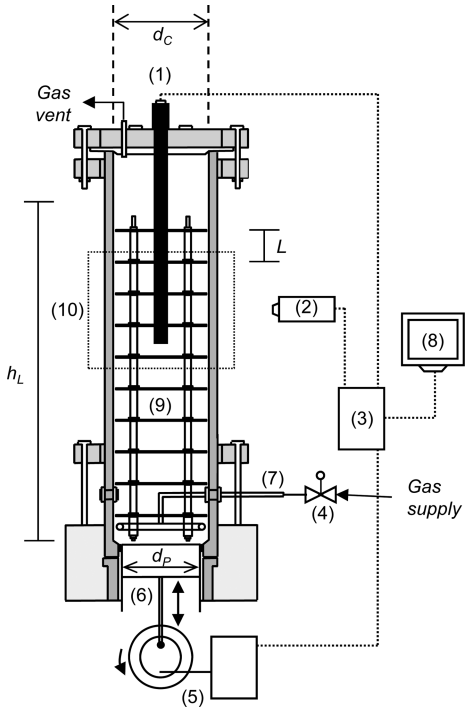

Figure 1. Configuration of the MOBC used for CO_2 mass transfer studies: (1) dissolved CO_2 probe; (2) CCD camera; (3) CPU; (4) gas flow controller (rotameter); (5) servo-hydraulic unit; (6) piston; (7) gas sparger; (8) display; (9) interbaffle cavity; (10) optical box (filled with glycerol). Dimensions were as follows: liquid height in column, h_L = 450 mm; interbaffle spacing, L = variable (specific of the baffle design tested; see Table 2 for more details); diameter of piston, d_P = 125 mm; maximum internal diameter of column, d_c = 150 mm.

the servo-hydraulic system, a maximum value of f = 8 Hz could be used with x_0 = 3 mm.

The batch oscillatory column was equipped with equally spaced multiorifice baffles with unique designs. Three stainless steel rods (6 mm diameter) were placed inside the column to support the set of baffles. Baffles were designed to fit closely to the column wall. Three different baffle configurations were used in this study (described as designs 1, 2, and 3), with significant differences in d_0 and α as detailed in Table 2. Design 1 was initially tested as it had been successfully applied to liquid–liquid systems and photochemical oxidation in recent times in the same column (unpublished data). The baffle design with d_o = 30 mm and α = 36% mimicked that of single-orifice OBCs used in liquid mixing studies.[12,13] Baffle designs 2 and 3 were developed using smaller values for d_o and α which were observed to be beneficial for enhancing gas–liquid contacting. In all experimental sets, baffles were stacked inside the column at an equal baffle spacing (L) of 50 mm (design 1 and 2) or 40 mm (design 3). The asymmetrical configuration of baffle designs 1 and 2, regarding holes distribution in the plate, resulted in selecting a value for L of 50 mm, which was selected based on other studies in MOBCs.[6,19,24] Design 3 aimed at replicating a set of single-orifice baffled tubes working at same peak oscillatory liquid flow velocity, where a stack of baffles is fixed and the liquid is moved by the action of a piston, following the OBC scale-up rule established by Smith and Mackley.[21] Thus, for baffle design 3 the value of L was adjusted to 40 mm on the basis of the optimization studies reported in literature,[15,23] which suggested L being in the range of 1.5–1.8 times the column diameter. This design used a fully symmetrical distribution of holes with a constant distance of 24 mm between any adjacent holes.

2.2. Flow Visualization and BSDs. For optical imaging of gas bubbles and particle tracing experiments in the MOBC, a Perspex-optical box was fitted at midheight of the MOBC and filled with glycerol as shown in Figure 1. The gap between the external and internal walls of the jacketed glass column was also filled with glycerol in order to reduce optical distortion.[25]

A fluorescent lamp attached to a light diffusor provided the necessary illumination for the tracking of bubble size using a low-speed (60 fps) or high-speed (1000 fps) CCD camera. For

Table 2. Configuration of the 3 Internal Baffle Designs Used in the MOBC

	Baffles design 1	Baffles design 2	Baffles design 3
	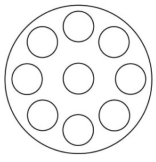	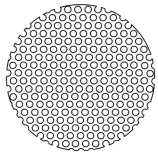	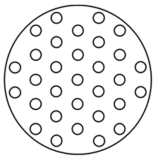
Number of baffles in the column	10	9	9
Average number of orifices per baffle	9	210	31
Orifice diameter d_o, mm	30.0	6.4	10.5
Equivalent diameter of obstacle d_{obs}, mm (Eq. 7)	40.0	7.9	24.8
Equivalent hydraulic diameter for single-orifice column d_h, mm (Eq. 10)	50.0	10.4	26.9
Baffle spacing L, mm	50	50	40
Baffle thickness	2.0	3.4	3.0
Open area α, %	36	42	15
Construction material for baffle	Stainless steel	Polypropylene sandwiched between 2 thin stainless steel layers	Acrylic

dx.doi.org/10.1021/ie403348g | Ind. Eng. Chem. Res. 2014, 53, 17303–17316

liquid flow visualization, polyamide particles having a mean size of 20 μm were dispersed in the liquid phase and illuminated at 90 deg to the camera by a mercury vapor lamp to give a bright illuminated field. A high-speed CCD camera (Photron FastCam) with a faster shutter speed was used to continuously acquire 512 × 512 pixels images. Images were saved to a PC in TIF format at a frequency of 1000 fps. A sequence of at least 600 image snapshots was taken at different combinations of x_0 and f, which provided more than 2000 bubbles for image analysis at each condition. This number of bubbles was concluded to be sufficient for the BSDs to be independent of the number of bubbles analyzed (results not shown).

Bubble image analysis was carried out using *ImageJ* software (NHI Image, USA). A set of 600 images for each experimental condition was converted to 8-bit binary images by applying a threshold. The binary images were then treated through a number of image processing steps in order to obtain a clear edge and area for each individual bubble, which included filling holes, erosion, and dilation. Finally, bubbles with minimum size higher than 0.02 mm^2 and circularity in the range of 0.7−1.0 were measured on the entire image sequence. Two important bubble diameters are usually relevant for gas−liquid mass transfer studies: the equivalent spherical bubble diameter (d_e) and the Sauter mean diameter ($D_{3,2}$). The size of each individual bubble was quantified from d_e which was calculated from the projected area (A_{proj}) according to eq 1:

$$d_e = \sqrt{\frac{4 \cdot A_{proj}}{\pi}} \tag{1}$$

In this equation it is assumed that all bubbles have spherical shape. This might had resulted in underestimated equivalent bubble size for the larger bubbles, which are less spherical and more likely to be oblate ellipsoids. Nevertheless, for the purpose of comparing baffle performances, the use of $D_{3,2}$ provides a good approximation and reduced error propagation from eq 1.

Given the restrictions in the flow visualization and postprocessing of the imaged bubbles, the minimum value of d_e that could be resolved was 0.16 mm. As CO_2 dissolution involved mass transfer through an interfacial area, $D_{3,2}$ was used and calculated using eq 2:

$$D_{3,2} = \frac{\sum_i {d_{e_i}}^3}{\sum_i {d_{e_i}}^2} \tag{2}$$

2.3. Measurement of K_La for CO_2 Dissolution. The dissolved CO_2 concentration in water was continuously monitored for each set of experiments using a dissolved CO_2 probe (InPro5000, Mettler Toledo) installed at a fixed position at the center of the MOBC, with the tip located at half-column height. Because of the large oscillatory Reynolds numbers used in this study, the estimate mixing times were in the range of few seconds[26] which is insignificant compared to the response time of the probe (150−180 s) and the long aeration times with 5% v/v CO_2 gas mixture. For that reason, the batch column was assumed to be well mixed.

The dynamic gassing-out method with instantaneous gas interchange, from pure nitrogen, N_2 to 5% CO_2 mixture was used to estimate K_La values for CO_2 in the batch MOBC. Before each set of experiments the column was filled with fresh distilled water. Nitrogen was then sparged for at least 60 min to promote degassing of the liquid and to set the reference 0% CO_2 saturation while starting data acquisition. The gas phase was then switched to a 5% v/v CO_2 mixture, and the gas flow rate was adjusted using a calibrated rotameter. The percentage saturation of dissolved CO_2 was then monitored until it reached a perfect plateau (i.e., 100% saturation). The pH electrode of the probe was calibrated in buffer at pH 7.00 and pH 9.21 as recommended by the manufacturer.

A time-lag on the dissolved CO_2 probe response was detected which was associated by other authors[10] with the time required for replacement of the gas in the connection tubing (connecting gas valves in the cylinder to the sparger), in the bubbles, in the liquid phase, and in the headspace. Consequently, a floating coordinate system ($t - t_0$), set as a constant for each gas flow rate used, was defined during data analysis, in which the time delay (t_0) was an arbitrary parameter determined by best-fitting the experimental data with the model using as objective function the minimum square of the difference. The value of t_0 determined for each Q_{gas} was within ±10% of the gas residence time that can be calculated on the basis of the gas flow rate, headspace volume, and gas holdups in the column.

To compensate for the effect of gas and liquid dynamics in the probe response, only values corresponding to 10−95% of the saturation dissolved CO_2 concentration (C_L*) were considered during the best-fitting procedure. According to Oliveira and Ni[27] a first order model and a step change in concentration technique can be used to evaluate the probe dynamics. Hence, the constant of the probe (K_P) was determined using a first order model in the column in a step change in CO_2 concentration, which could be determined from a mass balance to CO_2 dissolved in the liquid phase in the batch column:

$$\frac{C_L^* - C_L(t)}{C_L^* - C_{L,0}} = \exp(-K_P t) \tag{3}$$

The probe constants, K_P determined were 18 ± 2 h^{-1} for the set of experiments using baffle designs 1 and 2, and 23 ± 1 h^{-1} for the set of experiments shown with baffle design 3. These constants were different as these sets of experiments have been performed in different instances, and therefore some alteration to the membrane of the probe could have occurred.

Once the value of K_P was determined, it was then used to determine the volumetric CO_2−water mass transfer coefficient, K_La from the CO_2 dissolution plots, assuming a steady-state behavior for the gas dynamics (i.e., no significant decrease in partial pressure of CO_2 in the gas phase) and a perfectly mixed liquid phase. A mass balance to the gas phase combined with the first order model for probe dynamics defined in eq 3 yields

$$C_L(t) = C_L^* - \frac{C_L^* - C_{L,0}}{K_P - K_La}\{K_P \exp[-K_La(t - t_0)] - K_La \exp[-K_P(t - t_0)]\} \tag{4}$$

Equation 4 was then used to determine the K_La values for each experiment by best-fitting the experimental CO_2 dissolution profiles data to the model using Excel Solver, with the objective function being the minimum root-square difference between the two curves in the range of CO_2 saturation levels of 10−95% of C_L^*.

2.4. Modified Oscillatory Flow Dimensionless Numbers. In OBCs the oscillatory motion is complex[28] and traditionally the mixing intensity and mass transfer rates in the

dx.doi.org/10.1021/ie403348g | Ind. Eng. Chem. Res. 2014, 53, 17303−17316

Table 3. Averaged Bubble Sauter Mean Diameter ($D_{3,2}$) and Overall CO_2 Mass Transfer Coefficient (K_La) Values Obtained in the Different Baffle Designs

Q_{gas}	U_G	f	x_0					$D_{3,2}$	K_La
vvm	mm s^{-1}	Hz	mm	Re_o	Re'_o	St	St'	mm	h^{-1}
				Baffle Design 1					
0.05	0.43	0	0	0	0	*b*	*b*	5.51	9 (±1)
0.05	0.43	0.2	2.5	460	340	4.8	1.6	*a*	12 (±1)
0.05	0.43	3	1	2740	2030	11.9	4.0	5.28	*a*
0.05	0.43	3	2.5	6850	5070	4.8	1.6	5.41	*a*
0.05	0.43	3	5	13700	10140	2.4	0.8	*a*	9 (±2)
0.10	0.81	0	0	0	0	*b*	*b*	6.07	*a*
0.10	0.81	3	1	2740	2030	11.9	4.0	5.28	*a*
0.10	0.81	3	2.5	6850	5070	4.8	1.6	5.41	*a*
0.10	0.81	5	5	22830	16900	2.4	0.8	*a*	21
0.01	0.12	0	0	0	0	*b*	*b*	5.65	*a*
0.01	0.12	3	1	2740	2030	11.9	4.0	5.00	*a*
0.01	0.12	3	2.5	6850	5070	4.8	1.6	5.07	*a*
				Baffle Design 2					
0.10	0.81	0	0	0	0	*b*	*b*	3.23	48 (±7)
0.10	0.81	1	10	9130	1160	1.2	0.1	3.25	35 (±14)
0.10	0.81	2	10	18270	2310	1.2	0.1	2.33	*a*
0.10	0.81	4	5	18270	2310	2.4	0.2	2.59	20 (±10)
0.07	0.58	2	10	18270	2310	1.2	0.1	2.46	23 (±13)
0.04	0.35	2	10	18270	2310	1.2	0.1	2.43	4 (±1)
				Baffle Design 3					
0.10	0.81	0	0	0	0	*b*	*b*	*c*	20 (±1)
0.10	0.81	2	2	3650	4040	6.0	1.1	*c*	22
0.10	0.81	2	5	9130	10110	2.4	0.4	*c*	30
0.10	0.81	5	2	9130	10110	6.0	1.1	*c*	33 (±8)
0.10	0.81	4	3	10960	12130	4.0	0.7	*c*	37
0.10	0.81	5	3	13700	15160	4.0	0.7	*c*	43
0.10	0.81	2	8	14610	16170	1.5	0.3	*c*	45
0.10	0.81	8	2	14610	16170	6.0	1.1	*c*	57 (±9)
0.10	0.81	2	10	18270	20220	1.2	0.2	*c*	94
0.10	0.81	10	2	18270	20220	6.0	1.1	*c*	65 (±12)
0.10	0.81	7	3	19180	21230	4.0	0.7	*c*	48 (±1)
0.08	0.66	8	2	14610	16170	6.0	1.1	*c*	31 (±2)
0.06	0.50	8	2	14610	16170	6.0	1.1	*c*	27 (±3)
0.04	0.35	8	2	14610	16170	6.0	1.1	*c*	20
0.01	0.12	8	2	14610	16170	6.0	1.1	1.70	14
0.01	0.12	8	3	21920	24260	4.0	0.7	*a*	*a*
				Unbaffled Column					
0.10	0.81			no fluid oscillations				5.27	24 (±3)

[a]Not measured. [b]Strouhal number not applicable for steady flow. [c]Insufficient number of individual bubbles available for image analysis.

interbaffle regions of small diameter single-orifice OBCs is assumed as governed by two dimensionless numbers, the oscillatory Reynolds number (Re_o) and the Strouhal number (St):

$$Re_o = \frac{2\pi f x_0 \rho d_c}{\mu} \quad (5)$$

$$St = \frac{d_c}{4\pi x_0} \quad (6)$$

where d_c is the internal diameter of the column (m), f the fluid oscillation frequency (s^{-1}), μ is kinematic fluid viscosity (kg m^{-1} s^{-1}), ρ is the specific mass of the fluid (kg m^{-3}), and x_0 is the center-to-peak fluid oscillation amplitude (m).

The Re_o in eq 5 was described in analogy to net flow Reynolds number where the product $2\pi x_0 f$ represents the peak fluid velocity (m s^{-1}) during an oscillation cycle which occurs halfway through the piston full stroke. The St and Re_o dimensionless numbers in eqs 5 and 6 are routinely used in studies involving single-orifice OBCs in which there is a direct link between d_c and the open diameter of the orifice (d_o); however, they were found unsuitable for scaled-up OBCs and MOBCs for a number of reasons as follows.

A possible strategy for scale-up of OBCs from single-orifice columns is based on increasing the d_c by keeping both Re_o and St constant. Following from eq 6 this would require x_0 to be increased in proportion to d_c, and therefore for f to be reduced by 1−2 orders of magnitude in order to keep Re_o constant according to eq 5. This happens because currently Re_o on its current form is only based on d_c and not in d_o or the equivalent diameter of the obstacle (d_{obs}), as anticipated from a detailed understanding of the fluid mechanics behind flow separation around obstacles. An alternative and more elegant approach for

dx.doi.org/10.1021/ie403348g | Ind. Eng. Chem. Res. 2014, 53, 17303−17316

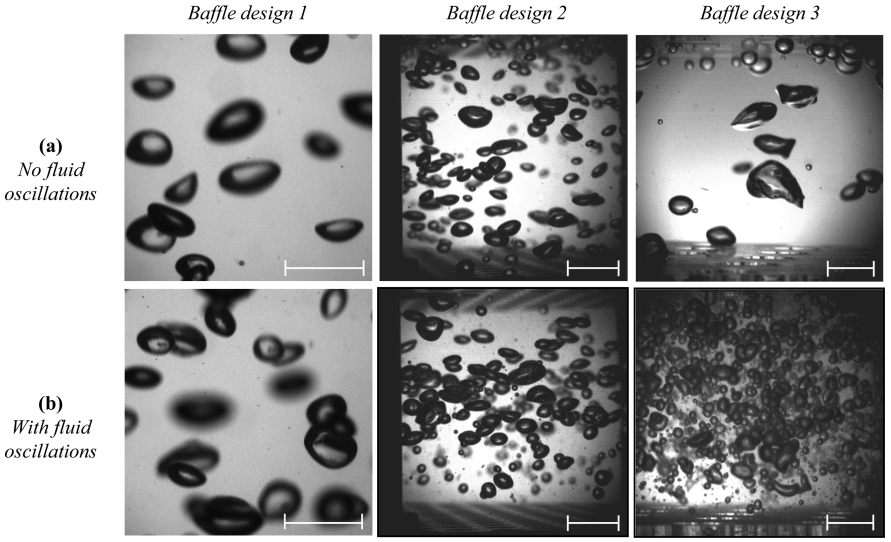

Figure 2. Optical observation of air bubbles rising in an interbaffle cavity in the vertical MOBC: (a) stagnant fluid; (b) oscillated fluid. The gas aeration rates, Q_{gas} and fluid oscillation conditions used were as follows. Baffle design 1: f = 3 Hz, x_0 = 2.5 mm, Re'_o = 5070, St' = 1.6, and Q_{gas} = 0.1 L min^{-1} (0.01 vvm). Baffle design 2: f = 2 Hz, x_0 = 10 mm, Re'_o = 2310, St' = 0.1, and Q_{gas} = 0.4 L min^{-1} (0.04 vvm). Baffle design 3: f = 2 Hz, x_0 = 10 mm, Re'_o = 20220, St' = 0.2, and Q_{gas} = 0.1 L min^{-1} (0.01 vvm). Scale bar corresponds to 10 mm.

scale-up of OBCs uses multiorifice baffles. With that approach, d_c is increased but both d_o and d_{obs} are kept constant. This is equivalent to multiple OBCs working effectively in parallel in the same column.

A number of variants to eq 5 was proposed by several authors for multiorifice baffles (see, for example, Ni and Gough,[29] Smith and Mackley[21]), yet the effect of α in the performance of MOBCs has not yet been considered. As this current study used baffles with a range of d_o and α both Re_o and St were modified to accurately represent the state of mixing in the MOBC and support scale-up from single-orifice to multiorifice OBCs.

Eddy formation in the free flow problem around obstacles is controlled by the diameter of the obstacle, the properties of the fluid, and the free mean liquid velocity. Therefore, the most important characteristic length in respect to vortices formation is d_{obs}, and in analogy it can be described for the MOBC as the "equivalent" diameter of the baffle area that surrounds each open orifice:

$$d_{obs} = d_c\sqrt{\frac{1-\alpha}{n}} \tag{7}$$

where n is the number of orifices in the baffle. For multiorifice baffles d_{obs} (not d_o or d_c as it happens for single-orifice OBCs) should be the main geometrical parameter governing flow separation and eddy formation in the column.

From the perspective of mass conservation, the flow of an incompressible fluid through a multiorifice baffle differs from a free-boundary flow problem because the fluid has to accelerate when passing through the orifices. Neglecting the effect of the column walls (because of the large d_c value the pseudosteady flow is turbulent in the interbaffle spaces), the mean free stream velocity relevant for vortices formation from the surface of the obstacles is not just controlled by the imposed mean fluid velocity (or peak fluid velocity $2\pi x_0 f$ in the case of unsteady flow) but also by α. Taking these simple concepts into account, a modified Re'_o for multiorifice baffles could be written as follows:

$$Re'_o = \left(\frac{2\pi f x_0 \rho}{\mu}\right) d_{obs}\left(\frac{1}{\alpha}\right) \tag{8}$$

Combining eqs 8 and 7 yields

$$Re'_o = \left(\frac{2\pi f x_0 \rho}{\mu}\right)\left(\frac{d_c}{\sqrt{n}}\right)\sqrt{\frac{1-\alpha}{\alpha^2}} \tag{9}$$

Mathematically eq 9 differs from the equation presented by Smith and Mackley[21] for a multiorifice OBC on the term $[(1-\alpha)/\alpha^2)^{1/2}]$ which measures the effect of the open area of the baffle. This yields significant differences in Re'_o values as can be seen in Table 3. For example, Re'_o calculated from eq 9 for baffle design 2 is about 8-fold lower than value of Re_o based on eq 5 because of the small value of d_o used.

Similarly, the Strouhal number St in eq 6 was modified to represent the actual ratio of diameter of column to fluid amplitude in the region around each individual orifice on the baffles in a MOBC. That required determining the equivalent hydraulic diameter of a single-orifice column, d_h:

$$d_h = \frac{d_c}{\sqrt{n}} \tag{10}$$

Replacing d_c in eq 6 by d_h from eq 10, gives a modified Strouhal number (St'):

$$St' = \frac{d_c}{4\pi x_0}\frac{1}{\sqrt{n}} \tag{11}$$

3. RESULTS AND DISCUSSION

3.1. The Impact of Q_{gas} and Fluid Oscillations on Bubble Size in the MOBC and Comparison with a Bubble Column. The $D_{3,2}$ and BSD are recognized as playing a major role in controlling K_La in gas−liquid and multiphase systems in single-orifice OBCs and other gas−liquid contacting systems, therefore the first part of this study aimed at testing the effect of Q_{gas} and fluid oscillations on the mean bubble size in the MOBC for selected multiorifice baffle designs. This was done using very low values of U_G of 0.12−0.81 mm s^{-1} which

dx.doi.org/10.1021/ie403348g | Ind. Eng. Chem. Res. 2014, 53, 17303−17316

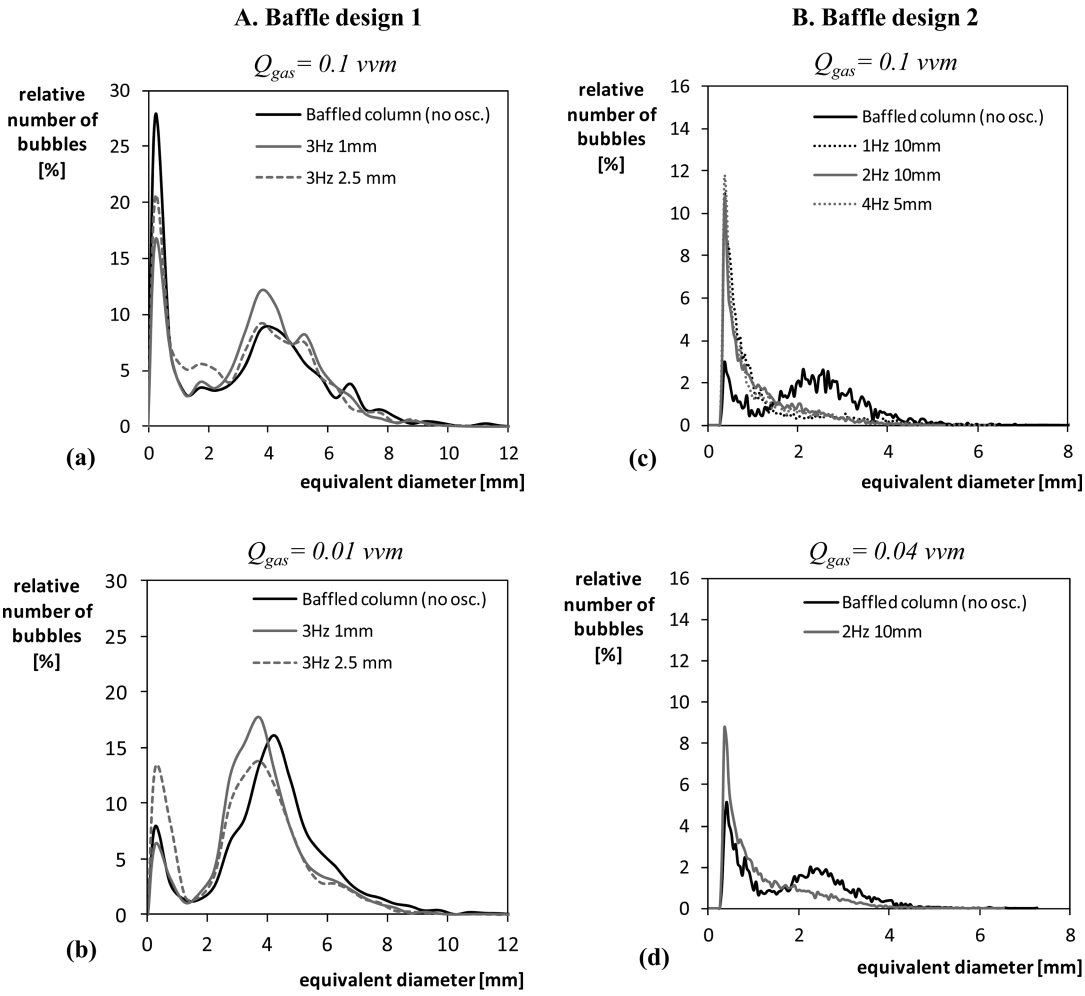

Figure 3. Bubble-size distributions in the MOBC fitted with (a–b) baffle design 1 or (c–d) baffle design 2.

are desirable to attain very high efficiencies of dissolution. Figure 2 shows the optical visualization of bubbles rising in the MOBC equipped with different sets of multiorifice baffles in the absence and presence of fluid oscillations. The mean bubble size was found strongly dependent on the baffle design; in particular, the small orifice diameter in design 2 (d_o = 6.4 mm, α = 42%) resulted in nearly 50% reduction in bubble size when compared to that of design 1 (d_o = 30 mm and α = 36%). Nevertheless, no trend could be observed with respect to the effect of intensity of fluid oscillations on the mean bubble size, as increasing Re_o' and St' for a given baffle design returned similar values for $D_{3,2}$ of ~5 or ~3 mm for baffle designs 1 and 2, respectively. With baffle designs 1 and 2 it was generally observed that the presence of the baffles *per se* had a stronger impact on bubble size than the intensity of the fluid oscillations on its own, as can be concluded by comparing the $D_{3,2}$ for each data set with the steady column baffled MOBC conditions (i.e., f = 0 Hz and x_0 = 0 mm) in Table 3. Baffle design 3 (d_o = 10.5 mm, α = 15%) with the smaller value of α produced an extremely large fraction of microbubbles, which is desirable for enhancement of gas–liquid mass transfer processes. Nevertheless, this presented a barrier for optical visualization of individual bubbles in the MOBC which is essential for calculating mean bubble sizes and BSDs even at such low values of U_G. For that reason it was not possible to collect systematically quantitative data about bubble size for Table 3. The three baffle geometries developed in this study aimed at covering the spectrum of orifice diameters and open areas previously used in single-orifice OBCs, and their impact on BSD is presented in more detail in Figures 3 and 4 for varying Q_{gas} values in a realistic number of experiments.

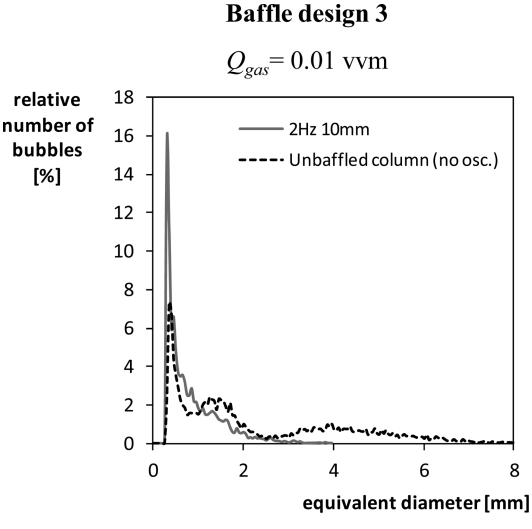

Figure 4. Bubble size distribution in the MOBC fitted with baffle design 3; comparison with unbaffled column.

dx.doi.org/10.1021/ie403348g | *Ind. Eng. Chem. Res.* 2014, 53, 17303–17316

The operation of the MOBC with baffle design 1 revealed a bimodal bubble population in the column (Figures 3a–b), with the first population having d_e < 1 mm, and the second bubble population having an average d_e around 4 mm. This bimodal population is typical in gas–liquid systems and results from the simultaneous bubbles coalescence and breakage phenomena occurring in the column. At the higher Q_{gas} of 0.1 vvm (Figure 3a) a number of fine bubbles in the range of few hundreds of micrometers could be detected in the column; however there was no significant difference between the MOBC and sparging the baffled column in the absence of fluid oscillations. This is illustrated in Figure 3a for two different combinations of fluid oscillations (f = 3 Hz, x_0 = 1 mm, St' = 4.0; and f = 3 Hz, x_0 = 2.5 mm, St' = 1.6). At a lower Q_{gas} = 0.01 vvm (Figure 3b), the effect of fluid oscillations remained unnoticed. The large d_o value used in baffle design 1 (i.e., 30 mm) was clearly ineffective in promoting radial mixing and bubble breakage in gas–liquid flow, consequently Q_{gas} was the main effect with respect to control of overall BSDs. This result was to some extent unexpected, as several studies using oscillatory flow mixing have previously shown enhanced bubble breakage for experiments performed with similar Q_{gas} but different single-orifice OBC designs.[30,31] This suggested that a correct length scale of d_o and d_{obs} combined with an even distribution of the orifices across the baffle are essential to promote effective eddy formation and achieve a desirable reduction in bubble sizes.

The BSDs obtained using baffle design 2 with d_o = 6.4 mm is shown in Figures 3c,d. Again, a bimodal distribution was observed for all experiments in the baffled vertical column in the absence of fluid oscillations at the gas flow rates tested, with a main population of larger bubbles with d_e in the range of 1.5–3 mm, and a second population composed of small bubbles having d_e < 1 mm. In the presence of fluid oscillations unimodal BSDs were produced for all values of Q_{gas} tested. In fact, in the presence of fluid oscillations, mainly submillimeter size bubbles were observed in the MOBC. A detailed optical observation of the CO_2 bubbles using a high-speed image recording showed that in certain phases of the oscillation cycle the fine bubbles moved in the opposite direction of the liquid flow, revealing strong secondary mixing and consequently bubbles being trapped within each interbaffle cavity for a fraction of the period of oscillation. This is expected to enhance contact time, and its overall impact with respect to K_La is discussed in detail in section 3.3.

In the presence of baffle design 3 (with d_o slightly larger but smaller α than baffle design 2) unimodal BSDs were observed in the presence of fluid oscillations, with virtually no bubbles larger than 1 mm to be observed in the column (Figure 4). For the range of Re_o' and St' tested it was not possible to accurately determine $D_{3,2}$ because virtually at all combinations of f and x_0 tested with this baffle design an extremely large number of microbubbles was generated even at the lowest value of Q_{gas}. At the highest values of Re_o' the liquid in the column turned opaque as a result of the extremely high number of microbubbles in the gas–liquid solution, which suggests enhanced gas–liquid contacting.

Figure 5 shows photographic images of bubbles at increasing Re_o' and a constant gas flow rate of Q_{gas} = 0.01 vvm when the MOBC was equipped with baffle design 3. A 68% reduction in $D_{3,2}$ was observed with fluid oscillations, at Re_o' = 16170 and St' = 1.1 (Figure 5b) and Re_o' = 24260 and St' = 0.7 (Figure 5c), compared with the unbaffled steady column. This significant reduction in $D_{3,2}$ at high values of Re_o' resulted in an increased

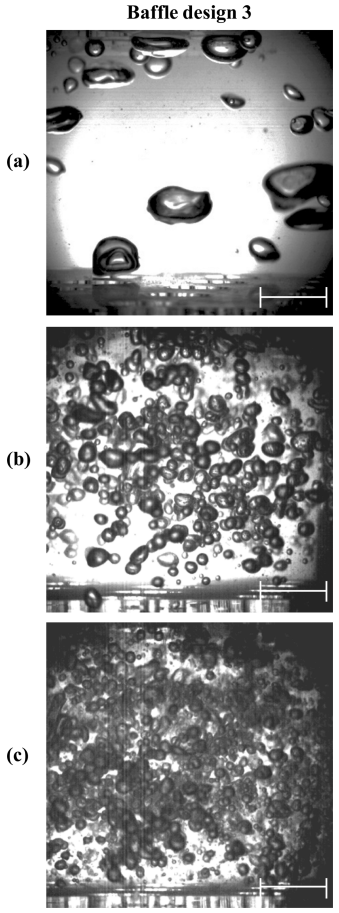

Figure 5. Impact of fluid oscillation conditions on bubble sizes in the MOBC configured with baffle design 3. (a) Re_o' = 0 (no fluid oscillations); (b) Re_o' = 16170, St' = 1.1, f = 8 Hz, and x_0 = 2 mm; (c) Re_o' = 24260, St' = 0.7, f = 8 Hz, and x_0 = 3 mm. Q_{gas} was kept constant at 0.1 L min^{-1} (0.01 vvm). The scale bar corresponds to 10 mm (the full image sequences are shown in film files supplied as Supporting Information).

interfacial area for mass transfer, which is an effective mean of enhancing mass transfer rates in the gas–liquid systems. The combination of a small d_o (as used by Reis et al.[30]) with high Re_o values (as used by Oliveira and Ni[31]) was apparently the central point for achieving a reduced mean size of bubbles in the MOBC. This can be briefly explained by recalling the physics behind drop generation in constricted flows as follows in section 3.2.

3.2. The Effect of Open Orifice Diameter and Simple Shear on Bubble Breakage. The breakup of liquid drops or gas bubbles can occur in constricted flows by the action of interfacial forces or inertial forces. Resulting from the very low viscosity of the liquid phase, the maximum capillary number calculated from the peak fluid velocities through the orifices in the three baffle designs tested was Ca = 0.012 (calculated for f = 7 Hz and x_0 = 3 mm), which usually indicates the interfacial forces should dominate the shear stresses. Nevertheless, the high Reynolds numbers of the fluid being forced through the orifices means the dynamics of fluid flow should be actually dominated by inertial effects. As mentioned in section 3.1 the presence of baffles *per se* was sufficient for reducing the mean size of bubbles, which suggested that the bubble breakup mechanism is mediated by inertial effects as the liquid and bubbles were pushed through the orifices. On such conditions,

dx.doi.org/10.1021/ie403348g | Ind. Eng. Chem. Res. 2014, 53, 17303–17316

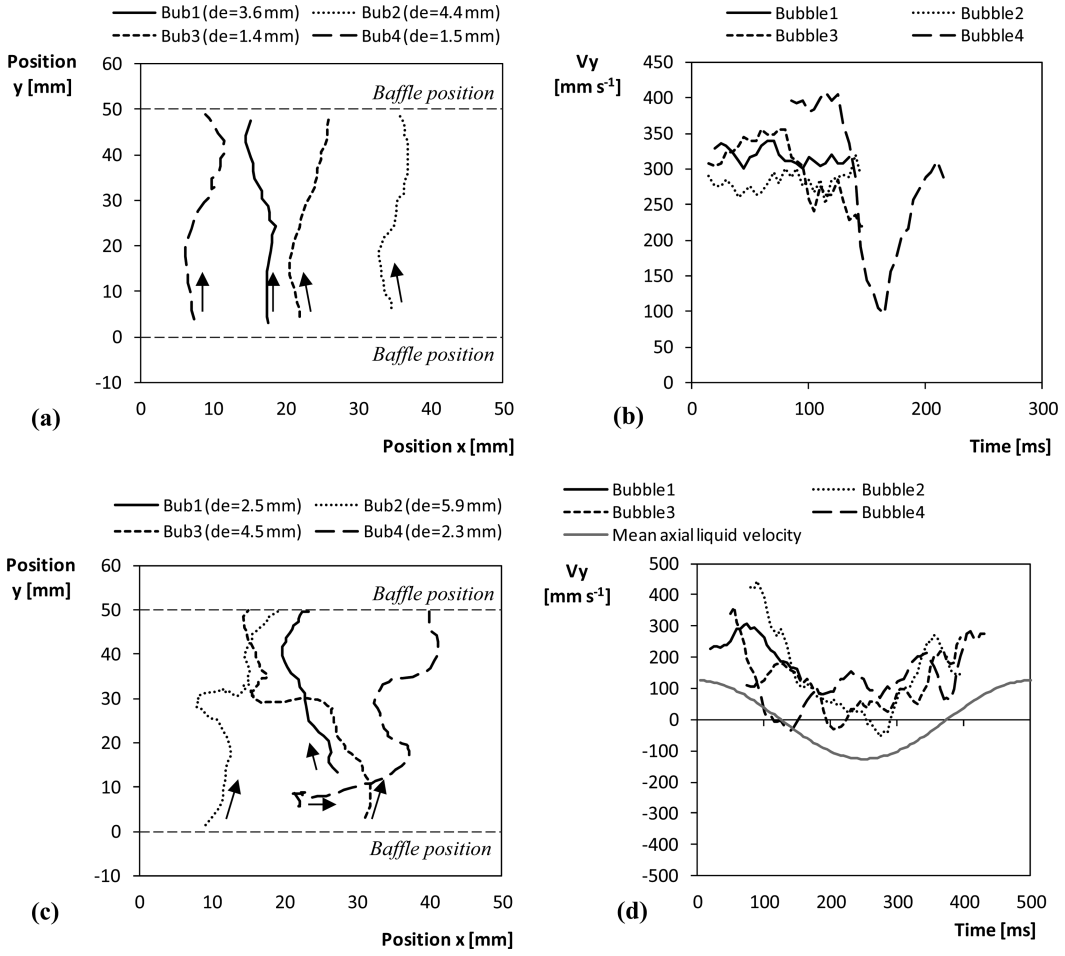

Figure 6. Time-tracking of (x,y) position and instantaneous vertical velocity (V_y) for four bubbles randomly selected in the interbaffle region in the MOBC configured with baffle design 2. The aeration rate was kept constant at 0.04 vvm. (a and b) stagnant column (i.e., $Re'_o = 0$); (c and d) fluid oscillated at $f = 2$ Hz, $x_0 = 10$ mm, $Re'_o = 2310$, $St' = 0.1$. Arrows in panels a and c show initial position and direction of the bubbles tracked.

the bubble breakup can be connected to the simple shear, $\dot{\gamma}_{SS}$ through an orifice with diameter d_o, which can be estimated from

$$\dot{\gamma}_{SS} = \frac{V_{mean}}{d_o} \tag{12a}$$

where V_{mean} is the peak fluid velocity through the orifice during the fluid oscillation, which can be directly calculated from the input f and x_0:

$$V_{mean} = 2\pi f x_0 \frac{1}{\alpha} \tag{12b}$$

Combining eqs 12a and 12b yields

$$\dot{\gamma}_{SS} = \frac{a}{\alpha d_o} \tag{13}$$

where $a = 2\pi f x_0$ and depends only on the fluid oscillation conditions selected. Equation 13 returned $\dot{\gamma}_{SS} = 93a$, $\dot{\gamma}_{SS} = 372a$ and $\dot{\gamma}_{SS} = 634a$ for baffle designs 1, 2, and 3, respectively. Comparatively, this represents a 4-fold increase in simple shear by replacing baffle design 1 with baffle design 2 (with smaller orifice size) and a 6.9-fold increase in $\dot{\gamma}_{SS}$ by replacing baffle design 1 with baffle design 3, which highlights the relevance of α and d_o on BSD. This also showed that $D_{3,2}$ is inversely proportional to the $\dot{\gamma}_{SS}$ agreeing with the traditional models for energy dissipation. Similar conclusions were also reported in other studies available in the literature.[6,19]

3.3. Flow Visualization of Liquid and Spatial Tracking of Bubbles in the MOBC. A further set of experiments used a high-speed camera for tracking the liquid flow and CO_2 bubbles in the MOBC equipped with baffle designs 2 or 3; design 1 was not analyzed as it underperformed with respect to BSD control as mentioned in section 3.1. First, the liquid phase was traced with polyamide particles, and an image sequence was recorded at 1000 fps. Photographic sequences taken in the MOBC equipped with baffle design 2 in three different positions of the oscillation cycle using $f = 4$ Hz and $x_0 = 5$ mm can be found in the Supporting Information (Figure S1). The area viewed corresponded to an entire interbaffle cavity (the position of the two baffles can be seen in the top and bottom of the figures). Although a range of values of Re'_o and St' was tested, baffle design 2 showed little evidence of strong eddy formation. The very large ratio $L/d_h = 4.8$ and the large number of orifices used in that particular baffle design presumably means the eddies were unable to reach the center of the cavity and the energy dissipation was limited to the edges of the orifices. The particle tracing experiments showed poor secondary eddy mixing through the oscillation cycle as fluid appeared to move only in straight lines in the direction of the piston stroke (Figure S1, in the Supporting Information). Although this baffle configuration delivered smaller bubbles sizes than design 1, it was also

dx.doi.org/10.1021/ie403348g | Ind. Eng. Chem. Res. 2014, 53, 17303−17316

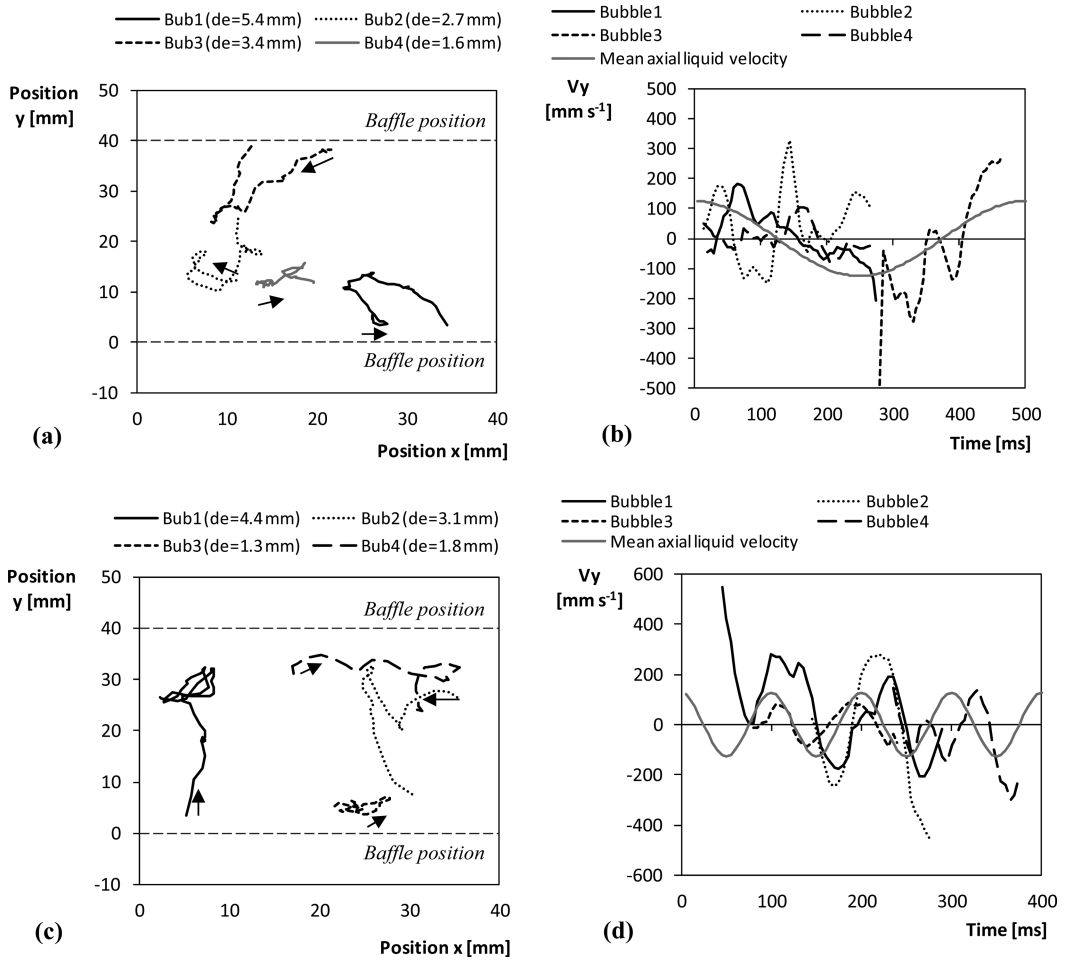

Figure 7. Time-tracking of (x,y) position and instantaneous vertical velocity (V_y) for four bubbles randomly selected in the interbaffle region in the MOBC configured with baffle design 3. The aeration rate was kept constant at 0.01 vvm. (a and b) obtained at f = 2 Hz, x_0 = 10 mm, Re'_o = 20220, St' = 0.2; (c and d) obtained at f = 10 Hz, x_0 = 2 mm, Re'_o = 20220, St' = 1.1. Arrows in panels a and c show initial position and direction of the bubbles tracked.

found inappropriate for the intensification of gas−liquid flows for presenting limited gas−liquid contacting (K_La values presented in section 3.4 were part of the basis of this final conclusion).

Optical flow visualization in the MOBC equipped with baffle design 3 showed very distinct liquid flow patterns. A photographic sequence of the liquid flow patterns in the interbaffle region (a pair of baffles can be seen on the top and bottom of the figures) with increasing Re'_o but approximately constant St' can be found in Supporting Information (Figure S2). Strong eddies were observed at different phases of the oscillation cycle and the intensity and size of eddies increased with increasing Re'_o as expected. At the highest value of Re'_o tested (Re'_o = 24260, f = 8 Hz, x_0 = 3 mm), the flow patterns revealed a mix of chaotic flow with well-defined toroidal vortices resulting in strong radial movement of the fluid, which is desirable for enhancing gas−liquid contacting and ultimately extend the contacting times in the column.

A second set of optical observations consisted in real-time tracking of bubbles in the MOBC. This was carried out only for baffle designs 2 and 3, and aimed to establish a qualitative link between gas-phase movement and the mass transfer performance. Figures 6 and 7 show on the left-hand side a tracking of the (x,y) position for a set of four bubbles randomly selected that could be observed rising through one interbaffle space, and on the right-hand side the instantaneous axial (vertical) velocity for each bubble corresponding to $V_y = \Delta y/\Delta t$ (mm s^{-1}). As a reference, the instantaneous mean fluid velocity imposed by the piston given by $V_y = 2\ \pi f x_0 \sin(2\pi f^* t)$ is also shown on the plots in Figures 6d, 7b, and 7d. The arrows in Figures 6a,c and 7a,c represent the direction and starting position of bubbles at the beginning of the tracking process. Using baffle design 2 and in the absence of fluid oscillations (Figure 6a−b), bubbles ascended the column with a mean instantaneous velocity of 300−350 mm s^{-1} which agrees well with the value for the terminal velocity of bubbles estimated from Stokes law in a bubble column.[32] In the presence of fluid oscillations (Figure 6c−d) there was some noticeable lateral displacement of the bubbles in the column which was an indicator of secondary or nonaxisymmetric flow being generated in the column. Analysis of V_y during an entire oscillation cycle (Figure 6d) has revealed two important facts. First, the rising velocity of bubbles varied throughout the oscillation cycle in a similar way to the liquid velocity and independently of the size of bubble selected. Second, V_y corresponded approximately to the net difference between the rising velocity in free flow (i.e., with no fluid oscillations, Figure 6b) and the instantaneous liquid flow velocity through the oscillation cycle. The V_y values were always positive, showing that bubbles were delayed when the oscillating piston was moving downward but accelerated as

dx.doi.org/10.1021/ie403348g | Ind. Eng. Chem. Res. 2014, 53, 17303−17316

the piston moved upward. This resulted in a net reduction in the residence time of the bubbles, therefore reducing contacting times in the column.

In respect to baffle design 3 the bubble tracking revealed something substantially different. Two combinations of frequency and amplitude for the same Re'_o = 20220 were presented in Figure 7 (f = 2 Hz, x_0 = 10 mm, St' = 0.2; f = 10 Hz, x_0 = 2 mm, St' = 1.1). The bubble tracking showed reduced vertical and increased lateral (radial) bubbles displacement in the interbaffle regions. This was associated with the strong radial mixing produced in the column by the formation of strong periodic eddies that are capable of trapping bubbles and overtake the natural buoyancy. Figure 7b,d showed bubbles effectively following the liquid flow in respect to space and time. At higher frequency (f = 10 Hz), bubbles could be seen trapped in the interbaffle regions for at least two full oscillation cycles (Figure 7d). This was due to the small open area of the baffles, which allowed effective generation of strong eddies throughout the oscillation cycle. In addition to a major reduction in $D_{3,2}$ reported in section 3.1 the contact time for mass transfer of CO_2 from the gas phase to the liquid phase in the column was also increased, which suggests larger mass transfer rates.

3.4. Effect of Fluid Oscillations on K_La. Table 3 summarizes K_La values obtained with the three different baffle configurations. The initial CO_2 dissolution trials using baffle designs 1 and 2 showed a marginal increase on K_La in the presence of fluid oscillations when compared to the unbaffled bubble column. This was associated with the large mean bubble sizes (design 1) and poor eddy mixing (design 2) observed in the MOBC. For that reason, only CO_2 dissolution using baffle design 3 is discussed in detail in this section. Before any comparison is made with K_La values available in the literature, it is important to highlight that the present study aimed at high CO_2 dissolution efficiencies, which involved using very low U_G values. At such values of U_G the mass transfer enhancement is usually challenging because of the very limiting interfacial area in a gas−liquid or multiphase system. Consequently, the K_La values obtained were somewhat smaller than the maximum K_La values reported by some authors for CO_2 and other gases[6,19,33] at much higher U_G values. Compared to the very few studies carried out at a similar range of U_G mean gas velocities used in this study (U_G = 0.12−0.81 mm s^{-1}) significant improvements could be observed in respect to K_La values. For example, in the study of Hewgill et al.,[13] using a O_2-water system, a range of K_La values of 7−13 h^{-1} can be estimated from the K_La versus U_G correlation reported (for U_G = 0.42−0.81 mm s^{-1}), which is 2 to 4 times lower than the K_La values obtained with the MOBC (14−57 h^{-1}).

Figure 8a summarizes the impact of baffles and fluid oscillations on CO_2 dissolution profile in the MOBC using baffle design 3. The required sparging time for 90% CO_2 saturation in the unbaffled column was observed as 14.5 min, and reduced to 12.8 min in the baffled (i.e., no fluid oscillations) column, while the use of "mild" (5 Hz, 2 mm) or "strong" (7 Hz, 3 mm) fluid oscillations reduced it further to 10.0 and 8.2 min, respectively. This represents up to 43% savings on CO_2−air mixture injected into the column in order to reach the same CO_2 saturation level. Despite fluid oscillations requiring external energy input that represents an additional cost to be considered, this type of mixing is energetically efficient as shown by power input studies in

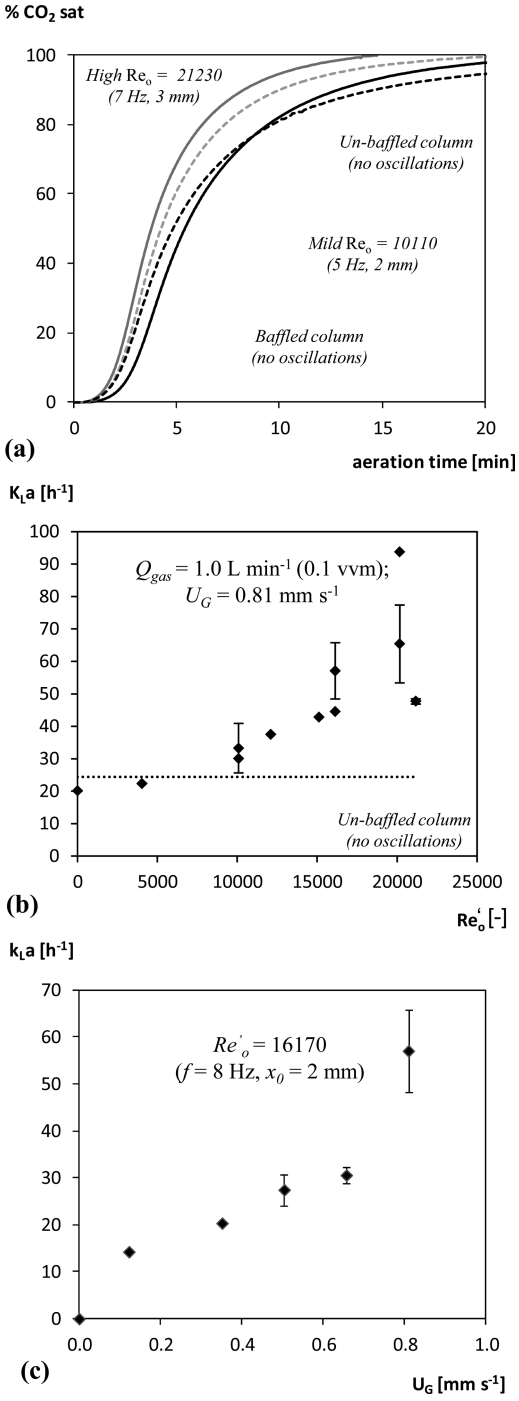

Figure 8. Effect of Re'_o and aeration rate U_G on the overall volumetric mass transfer coefficient K_La for the unbaffled and baffled multiorifice column using baffle design 3 (see Table 2 for more details). (a) Example of CO_2 dissolution profiles at a constant aeration rate Q_{gas} = 1.0 L min^{-1} (0.1 vvm) for different configurations and fluid oscillation conditions in the column; (b) variation of K_La with the modified oscillatory flow Reynolds number (Re'_o), at a constant flow rate Q_{gas} = 1.0 L min^{-1} (i.e., 0.1 vvm); (c) variation of K_La with mean superficial gas velocity (U_G) at a constant Re'_o = 16170, St' = 1.1, f = 8 Hz, x_0 = 2 mm. Error bars represent two standard deviations from experimental replicas.

OBCs; typical power inputs are in the range of 0.5−0.6 kW m^{-3} (see for example Baird et al.[12]).

In respect to K_La values, baffle design 3 revealed a major improvement in mass transfer rates when compared to the

dx.doi.org/10.1021/ie403348g | Ind. Eng. Chem. Res. 2014, 53, 17303−17316

other baffle designs initially explored. The K_La increased with an increase of both Re'_o and U_G as shown in Figure 8b,c. This agrees well with previous gas−liquid mass transfer studies using single-orifice OBCs[13,20,27] and a multiperforated reciprocating plate column.[19] A maximum value for K_La of 65 ± 12 h^{-1} was obtained at f = 2 Hz and x_0 = 10 mm, which corresponded to a 3.3- and 2.7-fold increase in K_La in comparison with steady "baffled" (K_La = 20 h^{-1}) column and "unbaffled" (K_La = 24 h^{-1}) column, respectively. The K_La values herein obtained were similar to those achieved by Taslim and Takriff[9] for a pure CO_2−water system, however with a 13- to 36-fold reduction in Q_{gas}.

It could also be observed in Figure 8b that the use of "gentle" fluid oscillations, at low values of f and x_0 (e.g., up to f = 2 Hz and x_0 = 2 mm in this study) were in general detrimental to the CO_2−water mass transfer process, as the values of K_La obtained at such conditions were slightly lower than the K_La values obtained with the unbaffled bubble column (dashed horizontal line in Figure 8b). This could be explained by the fact that "gentle" fluid oscillations generate very weak eddy vortices and a net acceleration of the bubbles during the piston stroke upward, as explained for bubble tracking experiments in section 3.3. The axial sinusoidal movement of the fluid leads to a net increase on the rising velocity of bubbles and consequently to reduced residence time of the bubbles in the column followed by a net drop on K_La. From Figure 8b a minimum value of Re'_o = 3000−4000 can be estimated to produce an effective increase in K_La. It was however not possible to confirm experimentally that the increase in K_La in the MOBC resulted from an enhancement in the gas−liquid contacting with increasing Re'_o value (i.e., mixing intensity) or from the change in the total interfacial area, as the cloudiness of the CO_2−water dispersions at higher Re'_o obstructed the direct optical measurement of individual bubble sizes. Nevertheless, the image sequences as presented in Figure 5 suggested that the increase in Re'_o resulted in no additional decrease in bubble size, instead increasing the number of bubbles in the interbaffle regions. This enhanced liquid mixing and yielded higher velocity fluctuations on the gas−liquid interface reducing the boundary layer on the bubble's surface, as previously shown in similar studies.[27,31]

In this study, it was found that K_La seems to vary linearly with Q_{gas} and U_G (Figure 8c). Other studies carried out in single-orifice OBCs of Oliveira and Ni,[27] Hewgill et al.,[13] and Taslim and Takriff[9] have shown a power law relationship between K_La and U_G, of the type obtained for bubble columns that could not be observed with baffle design 3. Al-Abduly et al.[34] and Hewgill et al.[13] obtained a relationship very close to the linearity. Gomaa et al.[33] compiled a set of eight correlations commonly used for K_La estimation of the type $K_La \propto U_G^b$, where b has a value in the range of 0.14−1.55. For one of those correlations b is close to unity, as it happens with the MOBC.

The high K_La values obtained for dissolution of CO_2 in water become relevant when considering the very low gas flow rates used (i.e., $Q_{gas} \leq 0.1$ vvm). For example, Hill[10] used a stirred tank reactor and Q_{gas} in the range of 0.08−0.80 vvm (i.e., up to 8 times higher aeration rates than in the current study) and achieved K_La values in the range of 20−120 h^{-1} (despite the conditions at which the highest K_La values have been obtained could not be determined from their work). That same study mentioned the best-fitted K_La value was obtained at 27.5 °C, 0.45 vvm and 375 rpm and was equal to 41.4 h^{-1}. Taslim and Takriff[8] performed similar CO_2 mass transfer studies in a single-orifice OBC and reported similar values for K_La, although working with very large Q_{gas} in the range of 1.3−3.6 vvm using pure CO_2. The high K_La values herein reported highlight the successful scale-up and high efficiency of CO_2 dissolution upon a proper baffled design in the MOBC. The fine gas−liquid dispersion with enhanced gas−liquid contacting times and improved K_La obtained in the MOBC equipped with baffle design 3 is unique with respect to efficiency of CO_2 dissolution.

4. CONCLUSIONS

Major improvements in K_La for CO_2 dissolution in water were reported for a MOBC working under oscillatory flow mixing and stagnant conditions. The K_La values reported of up to 65 ± 12 h^{-1} for very small superficial gas velocities below 1 mm s^{-1} were in the range of K_La values reported for other gas−liquid contacting systems operating at gas flow rates 10- to 40-fold higher. Baffle design showed a major impact in the performance of the gas−liquid contacting system with respect to $D_{3,2}$, BSD, and K_La control. The scale-up of baffle configurations from single-orifice OBCs required the even distribution of small diameter orifices and small aperture areas in order to generate a high degree of secondary mixing in the column; therefore, the main dimensionless numbers that govern oscillatory flow mixing have been redefined. The shear caused by the oscillatory flow in the highly constricted baffles resulted in the formation of monodispersed microbubbles. For the first time microbubble trapping by the strong toroidal vortices in the interbaffle regions was visually shown. The increased residence times and gas hold-ups caused by the retention of fine bubbles in the column combined with intensive oscillatory gas−liquid contacting were the main parameters responsible for the major increase obtained in K_La for CO_2. As significant K_La values were obtained with low U_G, the MOBC is an advantageous system for large-scale use in gas−liquid reactions and multiphase biotransformations. The results presented in this work are of general relevance to gas−liquid mass transfer in sparged systems and of particular relevance to bioreactor design for fermentation of C_1 compounds that will be the subject of future publications.

■ ASSOCIATED CONTENT

Supporting Information

Flow visualization films recorded with a high speed camera (relevant for baffle designs 2 and 3), supporting data shown in Figure 5. A text document is also provided with supplementary Figures S1 and S2, containing results from fluid particle tracking. This material is available free of charge via the Internet at http://pubs.acs.org

■ AUTHOR INFORMATION

Corresponding Author

*Tel. +44(0)1509 222 505. Fax +44 (0)1509 223 923. E-mail: n.m.reis@lboro.ac.uk.

Notes

The authors declare no competing financial interest.

■ ACKNOWLEDGMENTS

The authors acknowledge financial support of Fundação para a Ciência e Tecnologia (FCT) and the European Social Fund (ESF) through Ph.D. Grant SFRH/BD/62273/2009 awarded to F. M. Pereira. N. M. Reis is also grateful to the European

Commission through the Marie Curie programme and to BBSRC, UK, for financial support.

NOMENCLATURE

Abbreviations

fps = frames per second
rpm = rotations per minute
vvm = volume of gas per volume of liquid per minute
ss = simple shear

Symbols

a = mass transfer interfacial area (m^2)
A_{proj} = projected area of the bubble (mm^2)
$C_{L,0}$ = initial dissolved concentration (mg L^{-1})
C_L = dissolved CO_2 concentration (mg L^{-1})
C_L^* = concentration of saturation (mg L^{-1})
$D_{3,2}$ = Sauter mean diameter (mm)
d_c = internal diameter of the column (mm)
d_e = equivalent spherical diameter of bubble (mm)
d_h = equivalent hydraulic diameter for single-orifice column (mm)
d_o = orifice diameter (mm)
d_{obs} = equivalent diameter of the obstacle (mm)
d_p = diameter of piston (mm)
f = frequency of the oscillation (Hz)
h = height of the column (mm)
h_L = liquid height in the column (mm)
K_La = overall gas−liquid mass transfer coefficient (h^{-1})
K_P = constant of the probe (h^{-1})
L = spacing between baffles (mm)
n = number of orifices in the baffle (dimensionless)
Q_{gas} = gas aeration rate (vvm or L min^{-1})
Re_o = oscillatory Reynolds number (dimensionless)
Re_o' = modified oscillatory Reynolds number (dimensionless)
St = Strouhal number (dimensionless)
St' = Modified Strouhal number (dimensionless)
t = aeration time (s)
t_0 = time delay for the measuring of dissolved CO_2 concentration (s)
U_G = mean superficial gas velocity (mm s^{-1})
V_L = working liquid volume (L)
V_y = instantaneous axial (vertical) bubble or liquid velocity (mm s^{-1})
x_0 = center-to-peak amplitude of fluid oscillation (mm)
x_{CO_2} = CO_2 molar composition inlet gas (mol/mol)

Greek Letters

α = fraction of open area of the baffle (dimensionless)
Δt = time interval (s)
Δy = vertical displacement (mm)
μ = kinematic fluid viscosity (kg m^{-1} s^{-1})
ρ = specific mass of fluid (kg m^{-3})
$\dot{\gamma}$ = shear rate (s^{-1})

REFERENCES

(1) Ugwu, C. U.; Aoyagi, H.; Uchiyama, H. Photobioreactors for Mass Cultivation of Algae. *Bioresour. Technol.* **2008**, *99*, 4021−4028.
(2) Phillips, J. R.; Clausen, E. C.; Gaddy, J. L. Synthesis Gas as Substrate for the Biological Production of Fuels and Chemicals. *Appl. Biochem. Biotechnol.* **1994**, *45/46*, 145−157.
(3) Jansson, C.; Northen, T. Calcifying Cyanobacteria—The Potential of Biomineralization for Carbon Capture and Storage. *Curr. Opin. Biotechnol.* **2010**, *21*, 365−371.
(4) Klasson, K. T.; Ackerson, M. D.; Clausen, E. C.; Gaddy, J. L. Biological Conversion of Coal and Coal-Derived Synthesis Gas. *Fuel* **1993**, *72*, 1673−1678.
(5) Worden, R. M.; Grethlein, A. J.; Jain, M. K.; Datta, R. Production of Butanol and Ethanol from Synthesis Gas via Fermentation. *Fuel* **1991**, *70*, 875−884.
(6) Gagnon, H.; Lounès, M.; Thibault, J. Power Consumption and Mass Transfer in Agitated Gas−Liquid Columns: A Comparative Study. *Can. J. Chem. Eng.* **1998**, *76*, 379−389.
(7) Calderbank, P. H.; Lochiel, A. C. Mass Transfer Coefficients, Velocities and Shapes of Carbon Dioxide Bubbles in Free Rise through Distilled Water. *Chem. Eng. Sci.* **1964**, *19*, 485−503.
(8) Boogerd, F. C.; Bos, P.; Kuenen, J. G.; Heijnen, J. J.; van Der Lans, R. G. J. M. Oxygen and Carbon Dioxide Mass Transfer and the Aerobic, Autotrophic Cultivation of Moderate and Extreme Thermophiles: A Case Study Related to the Microbial Desulfurization of Coal. *Biotechnol. Bioeng.* **1990**, *35*, 1111−1119.
(9) Taslim; Takriff, M. S. Gas−Liquid Mass Transfer in Continuous Oscillatory Flow in a Baffled Column. *AJChE J.* **2004**, *4*, 1−6.
(10) Hill, G. A. Measurement of Overall Volumetric Mass Transfer Coefficients for Carbon Dioxide in a Well-Mixed Reactor Using a pH Probe. *Ind. Eng. Chem. Res.* **2006**, *45*, 5796−5800.
(11) Mackley, M. R.; Ni, X. Mixing and Dispersion in a Baffled Tube for Steady Laminar and Pulsatile Flow. *Chem. Eng. Sci.* **1991**, *46*, 3139−3151.
(12) Baird, M. H. I.; Rama Rao, N. V.; Stonestreet, P. Power Dissipation and Holdup in a Gassed Reciprocating Baffle-Plate Column. *Chem. Eng. Res. Des.* **1996**, *74*, 463−470.
(13) Hewgill, M. R.; Mackley, M. R.; Pandit, A. B.; Pannu, S. S. Enhancement of Gas−Liquid Mass Transfer Using Oscillatory Flow in a Baffled Tube. *Chem. Eng. Sci.* **1993**, *48*, 799−809.
(14) Mackley, M. R.; Stonestreet, P.; Thurston, N. C.; Wiseman, J. S. Evaluation of a Novel Self-Aerating, Oscillating Baffle Column. *Can. J. Chem. Eng.* **1998**, *76*, 5−10.
(15) Ni, X.; Gao, S. Scale-up Correlation for Mass Transfer Coefficients in Pulsed Baffled Reactors. *Chem. Eng. J.* **1996**, *63*, 157−166.
(16) Oliveira, M. S. N.; Fitch, A. W.; Ni, X. A Study of Bubble Velocity and Bubble Residence Time in a Gassed Oscillatory Baffled Column—Effect of Oscillation Frequency. *Chem. Eng. Res. Des.* **2003**, *81*, 233−242.
(17) Oliveira, M. S. N.; Fitch, A. W.; Ni, X.-W. A Study of Velocity and Residence Time of Single Bubbles in a Gassed Oscillatory Baffled Column: Effect of Oscillation Amplitude. *J. Chem. Technol. Biotechnol.* **2003**, *78*, 220−226.
(18) Oliveira, M. S. N.; Ni, X. Gas Hold-up and Bubble Diameters in a Gassed Oscillatory Baffled Column. *Chem. Eng. Sci.* **2001**, *56*, 6143−6148.
(19) Rama Rao, N. V.; Baird, M. H. I. Gas−Liquid Mass Transfer in a 15 cm Diameter Reciprocating Plate Column. *J. Chem. Technol. Biotechnol.* **2003**, *78*, 134−137.
(20) Reis, N.; Pereira, R. N.; Vicente, A. A.; Teixeira, J. A. Enhanced Gas−Liquid Mass Transfer of an Oscillatory Constricted-Tubular Reactor. *Ind. Eng. Chem. Res.* **2008**, *47*, 7190−7201.
(21) Smith, K. B.; Mackley, M. R. An Experimental Investigation into the Scale-up of Oscillatory Flow Mixing in Baffled Tubes. *Chem. Eng. Res. Des.* **2006**, *84*, 1001−1011.
(22) Ni, X.; Gao, S.; Cumming, R. H.; Pritchard, D. W. A Comparative Study of Mass Transfer in Yeast for a Batch Pulsed Baffled Bioreactor and a Stirred Tank Fermenter. *Chem. Eng. Sci.* **1995**, *50*, 2127−2136.
(23) Brunold, C. R.; Hunns, J. C. B.; Mackley, M. R.; Thompson, J. W. Experimental Observations on Flow Patterns and Energy Losses for Oscillatory Flow in Ducts Containing Sharp Edges. *Chem. Eng. Sci.* **1989**, *44*, 1227−1244.
(24) Vasic, B.; Bankovic-Ilic, I. B.; Lazic, M. L.; Veljkovic, V. B.; Skala, D. U. Oxygen Mass Transfer in a 16.6 cm i.d. Multiphase Reciprocating Plate Column. *J. Serbian Chem. Soc.* **2007**, *72*, 523−531.

(25) Reis, N.; Harvey, A. P.; Mackley, M. R.; Vicente, A. A.; Teixeira, J. A. Fluid Mechanics and Design Aspects of a Novel Oscillatory Flow Screening Mesoreactor. *Chem. Eng. Res. Des.* **2005**, *83*, 357−371.
(26) Mackley, M. R.; Dickens, A. W.; Williams, H. R. Experimental Residence Time Distribution Measurements for Unsteady Flow in Baffled Tubes. *Chem. Eng. Sci.* **1989**, *44*, 1471−1479.
(27) Oliveira, M. S. N.; Ni, X.-W. Effect of Hydrodynamics on Mass Transfer in a Gas−Liquid Oscillatory Baffled Column. *Chem. Eng. J.* **2004**, *99*, 59−68.
(28) Ni, X.; Mackley, M. R. Chemical Reaction in Batch Pulsatile Flow and Stirred Tank Reactors. *Chem. Eng. J.* **1993**, *52*, 107−114.
(29) Ni, X.; Gough, P. On the Discussion of the Dimensionless Groups Governing Oscillatory Flow in a Baffled Tube. *Chem. Eng. Sci.* **1997**, *52*, 3209−3212.
(30) Reis, N.; Mena, P. C.; Vicente, A. A.; Teixeira, J. A.; Rocha, F. The Intensification of Gas−Liquid Flows with a Periodic, Constricted Oscillatory-Meso Tube. *Chem. Eng. Sci.* **2007**, *62*, 7454−7462.
(31) Oliveira, M. S. N.; Ni, X.-W. Characterization of a Gas−Liquid OBC: Bubble Size and Gas Holdup. *AIChE J.* **2004**, *50*, 3019−3033.
(32) Talaia, M. A. R. Terminal Velocity of a Bubble Rise in a Liquid Column. *World Acad. Sci. Eng. Technol.* **2007**, *28*, 264−268.
(33) Gomaa, H. G.; Hashem, N.; Al-Taweel, A. M. Dispersion Characteristics and Mass Transfer in a Pilot-Scale Gas-Liquid Oscillatory-Plate Column. *Chem. Eng. Technol.* **2012**, *35*, 1300−1311.
(34) Al-Abduly, A.; Christensen, P.; Harvey, A.; Zahng, K. Characterization and Optimization of an Oscillatory Baffled Reactor (OBR) for Ozone−Water Mass Transfer. *Chem. Eng. Process. Process Intensif.* **2014**, *84*, 82−89.